Decomposing the dynamics of delayed networks: equilibria and rhythmic patterns in neural systems

Gábor Orosz[*]

* Department of Mechanical Engineering, University of Michigan, Ann Arbor, Michigan 48109 USA (e-mail: orosz@umich.edu).

Abstract: A method is presented that allows one to decompose the dynamics of networked dynamical systems with time-delayed coupling. The key idea is to "block-diagonalize" the system with the help of the eigenvectors of the coupling matrix. While large delayed networks are difficult to handle both analytically and numerically, the "small" blocks obtained by the decomposition can be investigated using standard methods. The proposed technique is applied to a neural network where the stability of the synchronized equilibria and periodic solutions are investigated. The methodology may also be applied for large engineered networks like electric power grids.

Keywords: delay, network, adjacency matrix, neuron, bifurcation

1. INTRODUCTION

Biological networks (e.g., neural networks) consist of interconnected elements and their emergent behavior is influenced by both the properties of individual elements as well as the couplings between those elements. Even though networks have been studied for many decades, most studies focused on the structure of networks; see Newman et al. (2006). While structure has a significant influence on the dynamics, one may observe many qualitatively different dynamical behaviors for a particular network architecture; see Orosz et al. (2009). Describing the dynamics of biological networks using mathematical models is a challenging task due to the large number of network elements and nonlinearities in the system and also due to the fact that the transmission of biological signals between elements involves elaborate biological processes. There exist mathematical models that describe the dynamics of network elements (e.g., neurons) using ordinary differential equations (ODEs) as well as the signal transmission processes using partial differential equations (PDEs), but these are usually only practical for small networks. On the other hand, there exist a class of models where only the network elements are modelled in detail and signal transmission is considered to be an instantaneous. The resulting ODEs can be applied for large networks but clearly neglect some important biochemical processes, and consequently, their capability to predict the global dynamics of the network (i.e., the time evolution of patterns of activity) is questionable.

In this paper, we consider a modeling framework where biological signal transmission is not modelled in detail but the time it takes to transmit the signal is accounted for using time delays. This approach results in delay differential equations (DDEs), which retain the essential infinite dimensionality of the dynamics while keeping the

models parsimonious, and so scalable for large networks. In physical systems, time delays usually lead to undesired behavior so engineers try to reduce them and/or use predictors to compensate the delay effects. In biology, delay reduction and state prediction may not possible but nature may in fact exploit time delays to change the arising patterns of activity when encoding/decoding information, performing computation or tuning regulatory mechanisms.

The mathematical tools presented in this paper exploit the structure of the network in order to decompose the dynamics. The resulting "small" systems can be analyzed with standard methods that allow us to decipher how delays influence the network dynamics. Similar decomposition techniques have been used to study the stability of equilibria in consensus networks (Lin and Jia (2009); Meng et al. (2011); Cepeda-Gomez and Olgac (2011)) and to investigate the stability of equilibria and periodic orbits for Hopf normal form oscillators (Choe et al. (2010); D'Huys et al. (2011)). Our goal here is to analyze equilibria, periodic motions and their interaction in neural networks where the oscillators are modeled with a general set of differential equations. For neural systems, stability of equilibria can be determined semi-analytically similarly to the above references, while the numerical techniques developed here are necessary for the analysis of periodic motions; that are used for encoding neural information.

2. DECOMPOSITION OF DELAYED NETWORKS

In this paper we consider a system consisting of N identical oscillators coupled by identical couplings

$$\dot{x}_i(t) = f\big(x_i(t)\big) + \frac{1}{N} \sum_{j=1}^{N} A_{ij}\, g\big(x_i(t), x_j(t-\tau)\big), \quad (1)$$

for $i = 1, \ldots, N$, where the internal state of node i is captured by the vector $x_i \in \mathbb{R}^n$ and the internal dynamics consist of a set of nonlinear ODEs $\dot{x}_i = f(x_i)$. The couplings are described by the function $g(x_i, x_j)$ that

depends on the states of the interacting nodes. The time delay τ is the time needed for the "unmodelled" signal transmission processes to take places (e.g., transmitting signals along the axons and dendrites in neural systems). The coupling structure of the system is captured by a directed graph, whose elements are represented by the coefficients of the N-dimensional interconnection matrix $A_N = [A_{ij}]$. Here we consider all-to-all coupling without self loops that is

$$A_{ij} = \begin{cases} 1 & \text{if} \quad j \neq i, \\ 0 & \text{if} \quad j = i, \end{cases} \tag{2}$$

but the decomposition method shown below is applicable for more general coupling architectures. Finally, in addition to the internal dynamics and couplings, one may consider external inputs which are omitted here for simplicity.

The dynamics of (1) may result in a variety of different behaviors. In particular, clustering states may arise where groups of neurons act in synchrony. Each cluster configuration corresponds to a subspace embedded in the $(n\,N)$-dimensional space. In this paper we will investigate a particular clustering, that is, full synchrony

$$x_i(t) = x_{\mathrm{s}}(t), \quad i = 1, \ldots, N. \tag{3}$$

Substituting (3) into (1) results in the delay differential equation (DDE)

$$\dot{x}_{\mathrm{s}}(t) = f\big(x_{\mathrm{s}}(t)\big) + \frac{M}{N}\, g\big(x_{\mathrm{s}}(t), x_{\mathrm{s}}(t - \tau)\big), \tag{4}$$

where

$$M = \sum_{j=1}^{N} A_{ij}, \tag{5}$$

that must be the same for every i to ensure the existence of synchronous solutions. For all-to-all coupling (2) we have $M = N - 1$. This equation may produce a variety of different behaviors, e.g., equilibria, periodic orbits, and even chaotic motion. Here we focus on the first two cases. Synchronized equilibria $x_{\mathrm{s}}(t) \equiv x_{\mathrm{s}}^*$ can be derived from

$$0 = f\big(x_{\mathrm{s}}^*\big) + \frac{M}{N}\, g\big(x_{\mathrm{s}}^*, x_{\mathrm{s}}^*\big), \tag{6}$$

that is, the delay does not influence the location of equilibria (but may influence their stability). On the other hand, periodic solutions can be found by solving the boundary value problem comprised of (4) and $x_{\mathrm{s}}(t) = x_{\mathrm{s}}(t + T_{\mathrm{p}})$. Indeed, the existence, shape and stability of periodic orbits are influenced by the delay. When analyzing a synchronized motion one must investigate the stability within the subspace (3) which is called *tangential stability*, and also the stability against perturbations that tend to break the synchronization, called *transversal stability*.

In order to linearize (1) about the synchronous solution (3) we define the perturbations

$$y_i = x_i - x_{\mathrm{s}}, \tag{7}$$

for $i = 1, \ldots, N$. Using Taylor expansion, the linearization of (1) can be written in the form

$$\dot{y}_i(t) = \Big(Df(x_s) + \frac{M}{N}\, D_1 g(x_s, x_s) \Big) y_i(t) \\ + \frac{1}{N} \sum_{j=1}^{N} A_{ij}\, D_2 g(x_s, x_s)\, y_j(t - \tau), \tag{8}$$

where the $n \times n$ matrices $Df(x_s), D_1 g(x_s, x_s), D_2 g(x_s, x_s)$ are time-independent when linearizing about an equi-

librium $x_{\mathrm{s}}(t) \equiv x_{\mathrm{s}}^*$. ($D_1$ and D_2 represent derivatives with respect to the first and second variables.) When linearizing about a periodic orbit $x_{\mathrm{s}}(t) = x_{\mathrm{s}}(t + T_{\mathrm{p}})$ the matrices become time-periodic with period T_{p}. Defining $\mathbf{y} = \mathrm{col}\,[\, y_1 \ y_2 \ \ldots \ y_N \,] \in \mathbb{R}^{nN}$ the linear system (8) can be rewritten as

$$\dot{\mathbf{y}}(t) = (I_N \otimes L)\, \mathbf{y}(t) + (A_N \otimes R)\, \mathbf{y}(t - \tau), \tag{9}$$

where

$$L = Df(x_s) + \frac{M}{N}\, D_1 g(x_s, x_s), \quad R = \frac{1}{N}\, D_2 g(x_s, x_s), \tag{10}$$

I_N is the N-dimensional unit matrix, and A_N is the adjacency matrix.

To decompose the system (9) we construct the coordinate transformation

$$\mathbf{y} = (T_N \otimes I)\mathbf{z} \tag{11}$$

where $\mathbf{z} = \mathrm{col}\,[\, z_1 \ z_2 \ \ldots \ z_N \,] \in \mathbb{R}^{nN}$, I is the $n \times n$ unit matrix, while $T_N = [\, e_1 \ e_2 \ \ldots \ e_N \,]$ where e_i is the i-th eigenvector of the adjacency matrix A_N. Using this transformation one may derive the linear mode equations

$$\dot{z}_i(t) = L\, z_i(t) + \Lambda_i R\, z_i(t - \tau), \quad i = 1, \ldots, N, \tag{12}$$

where Λ_i is the i-th eigenvalue of A_N. The obtained equations can be analyzed separately for each i using standard methods as will be demonstrated in the next section.

In particular, for all-to-all coupling (2), the eigenvalues of the adjacency matrix are

$$\Lambda_1 = N - 1, \quad \Lambda_i = -1, \quad i = 2, \ldots, N \tag{13}$$

and the corresponding eigenvectors are

$$e_1 = \begin{bmatrix} 1 \\ 1 \\ 1 \\ \vdots \\ 1 \end{bmatrix}, \ e_2 = \begin{bmatrix} 1 \\ -1 \\ 0 \\ \vdots \\ 0 \end{bmatrix}, \ e_3 = \begin{bmatrix} 1 \\ 0 \\ -1 \\ \vdots \\ 0 \end{bmatrix}, \cdots, e_N = \begin{bmatrix} 1 \\ 0 \\ \vdots \\ 0 \\ -1 \end{bmatrix}. \tag{14}$$

Thus the corresponding mode equations can be written as

$$\dot{z}_1(t) = L\, z_1(t) + (N - 1)R\, z_1(t - \tau), \\ \dot{z}_i(t) = L\, z_i(t) - R\, z_i(t - \tau), \quad i = 2, \ldots, N, \tag{15}$$

where the first equation (which is indeed the linearization of (4)) describes the tangential stability of the synchronized state while the second equation describes its transversal stability.

3. TYPE II NEUROMODELS

Mathematical models that describe the temporal dynamics of neurons are categorized as Type I or Type II; see Coombes (2008). Type I neurons display arbitrarily low firing frequencies at firing threshold, which quickly increase as the magnitude of the applied current is increased. Type II neurons, on the other hand, exhibit a nonzero, "critical" firing frequency at threshold and have a much shallower slope in terms of the frequency changes as a function of the applied current. Here we consider a Type II neuromodel, namely a Fitzhugh-Nagumo type model with direct electronic coupling (gap junctions):

$$Cv̇_i(t) = h\big(v_i(t)\big) - w_i(t) + I$$
$$+ \frac{1}{N}\sum_{j=1}^{N} A_{ij}\,\kappa\cdot\big(v_j(t-\tau) - v_i(t)\big)\,, \qquad (16)$$
$$ẇ_i(t) = v_i(t) - \gamma\,w_i(t)\,,$$

where

$$h(v_i) = v_i(1 - v_i)(v_i - a)\,. \qquad (17)$$

Here each neuron is described by two scalar variables, the membrane potential of the soma v_i and a so-called gating variable w_i which represents the ion transport trough the membrane. Comparing (16) with the general model (1) it is clear that $x_i = \mathrm{col}\,[\,v_i \quad w_i\,]$. The model also contains the following (scaled) parameters:

$$\begin{aligned} C &= 0.1 \quad\text{— membrane capacitance}\,,\\ I &= 0.5 \quad\text{— applied current}\,,\\ \gamma &= 0.5\,,\\ a &= 0.25\,. \end{aligned} \qquad (18)$$

Without coupling, i.e., for $\kappa = 0$, equations (16,17) with parameters (18) produce sustained oscillations of period $T_{\mathrm{p}} = 2.173$; see the stable periodic orbit in Fig. 1. The coupling term $\kappa\,\big(v_j(t-\tau) - v_i(t)\big)$ represents a direct electronic connection between the axon of the j-th neuron and the dendrites of the i-th neuron. Here $v_i(t)$ is the postsynaptic potential, $v_j(t-\tau)$ is the presynaptic potential, κ is the conductance of the gap junction and τ represents the signal propagation time along the axon of the j-th neuron (dendritic delays are omitted here). That is the presynaptic potential is equal to what the potential of the soma of the j-th neuron was τ time before.

Synchronous solutions are described by the equation

$$Cv̇_{\mathrm{s}}(t) = h\big(v_{\mathrm{s}}(t)\big) - w_{\mathrm{s}}(t) + I$$
$$+ \frac{M}{N}\kappa\big(v_{\mathrm{s}}(t-\tau) - v_{\mathrm{s}}(t)\big)\,, \qquad (19)$$
$$ẇ_{\mathrm{s}}(t) = v_{\mathrm{s}}(t) - \gamma\,w_{\mathrm{s}}(t)\,,$$

which is obtained by substituting $[\,v_i \quad w_i\,] = [\,v_{\mathrm{s}} \quad w_{\mathrm{s}}\,]$ $i = 1,\ldots,N$ into (16); cf. (3) and (4). Note that $M = N-1$ for all-to-all coupling.

When linearizing (16) about a synchronous state $[\,v_{\mathrm{s}} \quad w_{\mathrm{s}}\,]$ one obtains the matrixes

$$L = \begin{bmatrix} \frac{1}{C}h'(v_{\mathrm{s}}) - \frac{M}{N}\frac{\kappa}{C} & -\frac{1}{C}\\ 1 & -\gamma \end{bmatrix}, \quad R = \begin{bmatrix} \frac{1}{N}\frac{\kappa}{C} & 0\\ 0 & 0 \end{bmatrix}, \quad (20)$$

cf. (10). Substituting these into (15) one can determine the tangential and transversal stability of the synchronized state. Indeed the first equation of (15) with (20) gives the linerization of (19).

3.1 Stability of Equilibria

The synchronous equilibrium $x_{\mathrm{s}}^* = \mathrm{col}\,[\,v_{\mathrm{s}}^* \quad w_{\mathrm{s}}^*\,]$ is given by the algebraic equations

$$\begin{aligned} 0 &= h(v_{\mathrm{s}}^*) - w_{\mathrm{s}}^* + I\,,\\ 0 &= v_{\mathrm{s}}^* - \gamma\,w_{\mathrm{s}}^*\,, \end{aligned} \qquad (21)$$

cf. (6). One may notice that the coupling term disappears and consequently the synchronized equilibrium is the same as the equilibrium of an uncoupled neuron. For parameters (18), we have a unique equilibrium as shown by the red dot in Fig. 1(b) at the intersection of the gray nullclines given by (21).
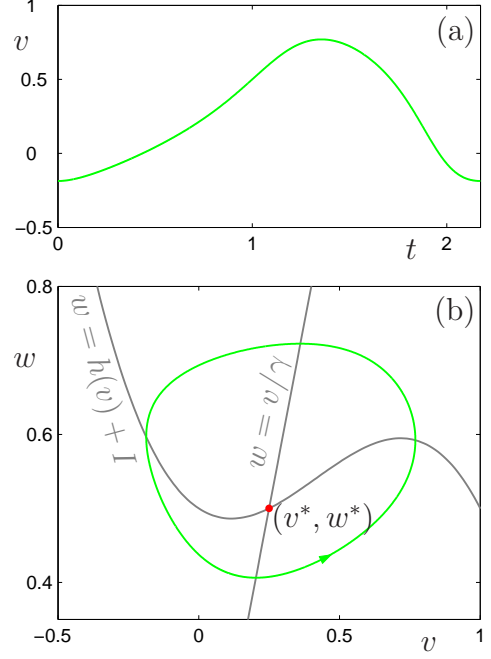

Fig. 1. Stable periodic solution of model (16) for parameters (18) without coupling $\kappa = 0$. Panel (a) shows the variation of the voltage v as a function of time t while panel (b) depicts the periodic orbit in state space where the equilibrium $(v^*, w^*) = (0.25, 0.5)$ is unstable.

In order to determine the tangential and transversal stability of the equilibrium, one must evaluate the matrixes (20) at $[\,v_{\mathrm{s}}^* \quad w_{\mathrm{s}}^*\,]$. Substituting the result into (15) and using the notation $z_1 = z_{\mathrm{s}} = [\,\tilde{v}_{\mathrm{s}} \quad \tilde{w}_{\mathrm{s}}\,]$ and $z_i = z_{\mathrm{b}} = [\,\tilde{v}_{\mathrm{b}} \quad \tilde{w}_{\mathrm{b}}\,]$, $i = 1,\ldots,N$, we obtain the equations

$$\begin{bmatrix} \dot{\tilde{v}}_{\mathrm{s}}(t)\\ \dot{\tilde{w}}_{\mathrm{s}}(t) \end{bmatrix} = \begin{bmatrix} -p - q & -\frac{1}{C}\\ 1 & -\gamma \end{bmatrix} \begin{bmatrix} \tilde{v}_{\mathrm{s}}(t)\\ \tilde{w}_{\mathrm{s}}(t) \end{bmatrix} + \begin{bmatrix} q & 0\\ 0 & 0 \end{bmatrix} \begin{bmatrix} \tilde{v}_{\mathrm{s}}(t-\tau)\\ \tilde{w}_{\mathrm{s}}(t-\tau) \end{bmatrix},$$
$$(22)$$

and

$$\begin{bmatrix} \dot{\tilde{v}}_{\mathrm{b}}(t)\\ \dot{\tilde{w}}_{\mathrm{b}}(t) \end{bmatrix} = \begin{bmatrix} -p - q & -\frac{1}{C}\\ 1 & -\gamma \end{bmatrix} \begin{bmatrix} \tilde{v}_{\mathrm{b}}(t)\\ \tilde{w}_{\mathrm{b}}(t) \end{bmatrix} + \begin{bmatrix} -r & 0\\ 0 & 0 \end{bmatrix} \begin{bmatrix} \tilde{v}_{\mathrm{b}}(t-\tau)\\ \tilde{w}_{\mathrm{b}}(t-\tau) \end{bmatrix},$$
$$(23)$$

where

$$\begin{aligned} p &= -\frac{1}{C}h'(v_{\mathrm{s}}^*) = \frac{1}{C}\big(3(v_{\mathrm{s}}^*)^2 - 2(a+1)v_{\mathrm{s}}^* + a\big)\,,\\ q &= \frac{N-1}{N}\frac{\kappa}{C}\,,\\ r &= \frac{1}{N}\frac{\kappa}{C}\,. \end{aligned} \qquad (24)$$

The subscripts s and b refer to synchronous and synchrony braking perturbations.

In order to determine the stability of equilibria we substitute trial solutions ($\sim \mathrm{e}^{\lambda t}, \lambda \in \mathbb{C}$) into (22) and (23). The corresponding characteristic equations are

$$\big(\lambda + p + q(1 - \mathrm{e}^{-\lambda\tau})\big)(\lambda + \gamma) + \frac{1}{C} = 0\,, \qquad (25)$$

and

$$\big(\lambda + p + q + r\mathrm{e}^{-\lambda\tau})\big)(\lambda + \gamma) + \frac{1}{C} = 0\,. \qquad (26)$$

The equilibrium is tangentially/transversally stable when all the infinitely many λ solutions of (25)/(26) are located

in the left-half complex plane. To find the stability boundaries we substitute $\lambda = \mathrm{i}\omega$ into (25) and (26), separate the real and imaginary parts, and after some algebraic manipulation we obtain the boundaries for tangential stability

$$\tau = \frac{2}{\omega}\left(\arctan\left[\frac{\beta}{\alpha}\right] + \ell\pi\right), \quad \ell = 0, 1, 2\ldots$$
$$\kappa = -\frac{CN}{2(N-1)}\frac{\delta}{\beta}, \tag{27}$$

and for transversal stability

$$\tau = \frac{2}{\omega}\left(\arctan\left[\frac{-\beta/\alpha \pm \sqrt{\beta^2/\alpha^2 - (N-2)}}{N-2}\right] + \ell\pi\right),$$
$$\ell = 0, 1, 2\ldots$$
$$\kappa = \frac{C}{N-2}\left(-(N-1)\beta \pm \sqrt{(N-1)^2\beta^2 - (N-2)\delta}\right), \tag{28}$$

where

$$\alpha = \omega - \frac{1}{C}\frac{\omega}{\gamma^2 + \omega^2},$$
$$\beta = p + \frac{1}{C}\frac{\gamma}{\gamma^2 + \omega^2}, \tag{29}$$
$$\delta = p^2 + \omega^2 + \frac{1}{C}\frac{1}{\gamma^2 + \omega^2}\left(\frac{1}{C} + 2p\gamma - 2\omega^2\right).$$

The corresponding curves are plotted for $N = 33$ in the (τ, κ)-plane in Fig. 2(a). These are parameterized by the angular frequency ω as shown by the green and red arrows. The curves for tangential stability (27) form lobes and the angular frequency along the lobes changes form $\omega = \pi/2$ to $\omega \to \infty$ as shown by the green arrows in panel (a) and the green curve in panel (b). Notice that the the tip of the lobes are at $\omega \approx \pi$. For transversal stability boundaries (28) form a single horizontal curve in the (τ, κ)-plane; see Fig. 2(a). Along this curve the angular frequency varies in a narrow frequency domain around $\omega \approx \pi$ as shown by the red arrows in panel (a) and the red circle in panels (b,c). The stability of the synchronized equilibrium changes via Andronov-Hopf bifurcation when crossing either a tangential or a transversal stability curve. That is a pair of complex conjugate eigenvalues crosses the imaginary axis. The angular frequency of the arising oscillations are approximated by the imaginary part of the crossing roots ω. Depending on whether tangential or transversal stability curve is crossed the arising spatiotemporal patterns will differ.

Considering (25) and applying the analytical stability criteria by Stépán (1989), it can be shown that the system is tangentially stable within in the leftmost lobe. Similar investigations for (26) reveal that the system is transversally stable above wavy curve. For stability, both tangential and transversal stability is required which is only satisfied in the shaded domain in Fig. 2(a). We remark that when increasing the number of neurons the lobes as well as the wavy curve move downward while the "amplitude" of the wavy curve decreases. However, $N = 33$ is already very close to the limit $N \to \infty$, that is, no significant changes observed when increasing N further.
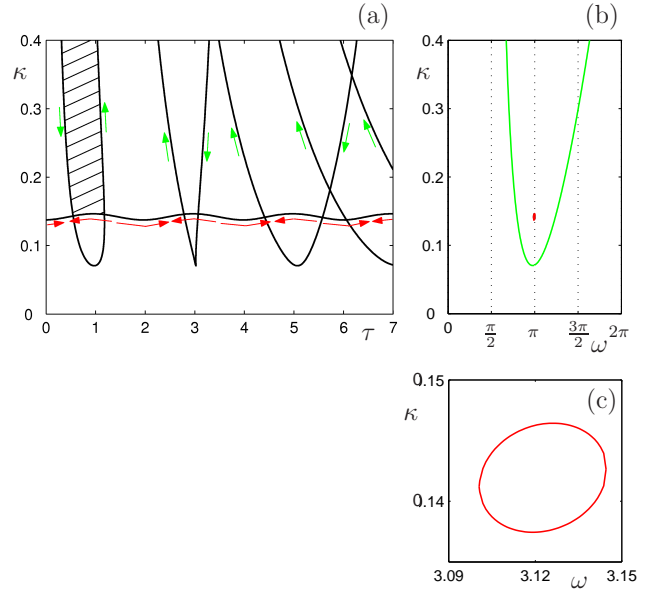

Fig. 2. Panel (a) depicts the stability chart representing changes in tangential stability (lobes) and transversal stability (horizontal curve) of the synchronized equilibrium. The green and red arrows show the variation of angular frequency ω along the curves. This change is also represented in panel (b) and a zoom is shown in panel(c).

3.2 Stability of Periodic Orbits

As shown above, decomposing system (16) allows one to determine the stability of equilibria in a systematic way. However, neural systems encode information using rhythmic patterns which usually corresponds to periodic orbits. To obtain synchronous periodic solutions, one must solve (19) considering $[\,v_\mathrm{s}(t) \quad w_\mathrm{s}(t)\,] = [\,v_\mathrm{s}(t + T_\mathrm{p}) \quad w_\mathrm{s}(t + T_\mathrm{p})\,]$ where T_p is the period of oscillations. To obtain these solutions we use numerical continuation (Roose and Szalai (2007)), namely the package DDE-BIFTOOL (Engelborghs et al. (2001)). In this case, a periodic orbit is represented on a discrete mesh and the solution between mesh points is approximated using low-order polynomials; see already Fig. 4. This method requires an "initial guess" of the solution for a particular parameter value, which may be obtained by numerical simulation. Then the Newton-Raphson method is applied to correct the solution. The obtained solution can also be used as a prediction for nearby parameter values. This allows us to follow branches of periodic solutions when varying parameters; see already Fig. 3. Our goal is to calculate the periodic solutions and also their stability for different values of τ and κ, and generate stability charts for the periodic solutions.

When linearizing (16) about synchronous oscillations, the matrices (20) must be evaluated at the periodic orbits. Consequently, L becomes time dependent through $h'(v_\mathrm{s}(t))$. (For more general couplings, R may also become time dependent.) Equations (22) and (23) can still be used to determine the tangential and transversal stability when considering $p(t) = -h'(v_\mathrm{s}(t))/C$. However, instead of exponential trial solutions one must use Floquet theory to determine the stability; see Insperger and Stépán (2011). The states $z_{\mathrm{s},t}(\theta) = z_\mathrm{s}(t + \theta)$ and $z_{\mathrm{b},t}(\theta) = z_\mathrm{b}(t + \theta)$,
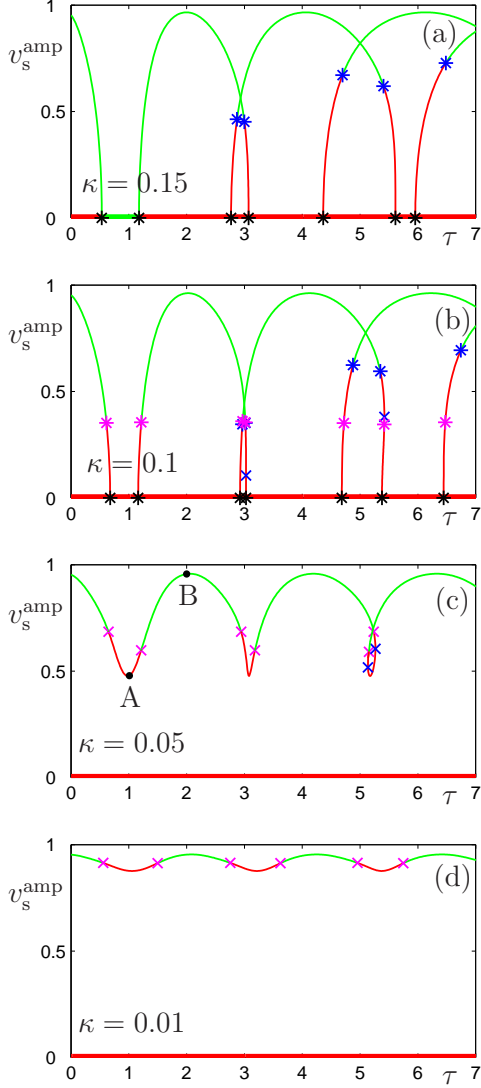
Fig. 3. Bifurcation diagrams showing the peak-to-peak voltage amplitude of synchronized oscillations as a function of the delay τ for different values of the coupling strength κ. The horizontal axis represent the equilibrium. Stable and unstable states are depicted by green and red curves. Black stars represent the Hopf bifurcations of equilibria while blue and magenta stars represent tangential and transversal Neimark-Sacker bifurcations of periodic orbits, respectively. Tangential fold and transversal pitchfork bifurcations are denoted by blue and magenta crosses, respectively.

$\theta \in [-\tau, 0]$ that are contained by the infinite-dimensional space of continuous functions can be obtained from the initial functions by solution operators

$$z_{s,t} = \mathcal{U}_s(t)\, z_{s,0}\,, \qquad z_{b,t} = \mathcal{U}_b(t)\, z_{b,0}\,. \qquad (30)$$

The nonzero elements of the monodromy operators $\mathcal{U}_s(T_p)$ and $\mathcal{U}_b(T_p)$, called Floquet multipliers, determine the tangential and transversal stability of oscillations. If all these multipliers are smaller than 1 in magnitude, the periodic solution is stable. The tangential eigenvalues are available in DDE-BIFTOOL since these come from (22) which is the linearization of (19). On the other hand, to obtain the transversal eigenvalues one need to evaluate the matrices in (23) at the solutions obtained from (19).
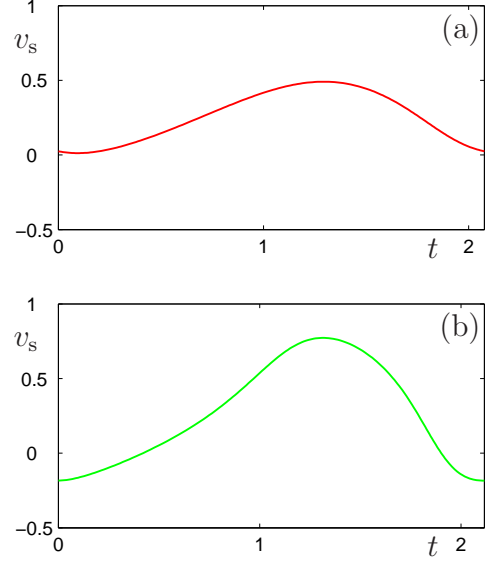

Fig. 4. Stable and unstable periodic orbits corresponding to the point A and B marked on Fig. 4(c).

Fig. 3 shows the peak-to-peak voltage amplitude of the oscillations when the time delay τ is varied. The corresponding value of the coupling constant is spelled out in each panel. Stable and unstable oscillations are depicted as green and red curves, respectively, and the same color code is used for the equilibrium (horizontal axis). Fold and pitchfork bifurcations (when a real multiplier crosses the unit circle at 1) are marked by crosses, while Neimark-Sacker bifurcations (when a complex conjugate pair of multipliers crosses the unit circle) are marked by stars. Blue and magenta symbols represent tangential and transversal stability losses.

For week coupling (Fig. 3(d)) the amplitude of oscillations does not change significantly and stability is lost via transversal pitchfork bifurcations (magenta crosses). Branches of symmetry-braking periodic solutions arise through these bifurcations (that are not shown in the figure). As the coupling strength is increased (Fig. 3(c)), tangential fold bifurcations (blue crosses) appear for larger delay values and the amplitude varies significantly with the delay. In particular, the amplitude of unstable oscillations decreases, which can also be observed in Fig. 4, depicting unstable and stable oscillations corresponding to the points A and B. When the coupling strength exceeds the minimum of the lobes in Fig. 2(a), the periodic branches "touch the ground" and connect to the equilibrium branch via Hopf bifurcations (black start); see Fig. 3(b). Also, in this domain both tangential and transversal stability losses occur mostly via Neimark-Sacker bifurcations (blue and magenta stars). At these bifurcations branches of quasi-periodic oscillations are created (not shown in the figure) that lead to complicated spatiotemporal patterns. Finally, when the coupling strength exceed the maximum of the wavy curve in Fig. 2(a), all transversal bifurcations disappear an only tangential Neimark-Sacker bifurcations remain; see Fig. 3(a). For large delays the arising quasi-periodic oscillations may undergo further bifurcations leading to synchronized chaos; see Choe et al. (2010) and D'Huys et al. (2011).
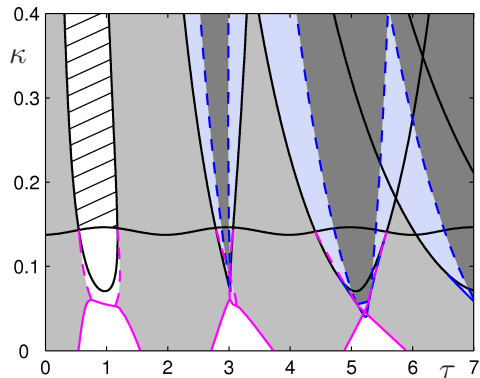
Fig. 5. Stability charts for synchronous periodic orbits. Black curves show the locations of Hopf bifurcations of equilibria; c.f. Fig. 2(a). Dashed blue and dashed magenta curves represent tangential and transversal Neimark-Sacker bifurcations, respectively. Solid blue curves represent tangential fold while solid magenta curves represent transversal pitchfork bifurcations.

All bifurcations of equilibria and periodic orbits are summarized in Fig. 5. Hopf bifurcations of the equilibrium are shown as black curves and the domain where the equilibrium is stable is shaded; cf. Fig. 2(a). Tangential bifurcations of periodic motion are shown as blue curves that are solid for fold and dashed for Neimark-Sacker bifurcations. Similarly magenta curves represent transversal pitchfork (solid) and Neimark-Sacker (dashed) bifurcations. Notice that as κ is increased the transversal bifurcations "switch" from pitchfork to Neimark-Sacker trough bifurcations of higher codimension. In the white regions only unstable oscillations exist. Bright gray regions contain one stable while dark gray regions contain two stable periodic orbits. In the light blue regions stable and unstable oscillations coexist.

We remark that for weak coupling one might reduce system (16) to a systems of coupled phase oscillators; see Izhikevich (1998). However, this approach does not provide information about the amplitude variations and only predicts transversal pitchfork instabilities; see Montbrió et al. (2006). In fact, the phase oscillator model predicts the first trapezoidal shaped domain in Fig. 5 as a triangle, while in reality the top of the triangle is "chopped off".

4. CONCLUSION

In this paper we have presented a decomposition method that can be used to analyze the dynamics of delayed networks. The method has been applied to analyze equilibria and periodic rhythms of neural networks consisting of identical, type II neurons. In particular, the synchronous state was analyzed and it was found that the equilibrium can lose stability via tangential and transversal Hopf bifurcations. The former one leads to oscillatory motion where the neurons remain synchronized while in the latter case synchrony is broken during oscillations. Similarly, synchronous oscillations may lose stability via (tangential and transversal) fold, pitchfork and Neimark-Sacker bifurcations, creating synchronous and non-synchronous oscillations that may be periodic or quasi-periodic. Our results demonstrate that time delays have a huge impact on the emergent dynamics of networks and can generate a very rich spatiotemporal behavior. As future research directions we aim to extend the decomposition method for cluster states and apply it to networks containing heterogeneities (non-identical elements, couplings and delays). Moreover, other applications, like electric power grids, will be considered.

REFERENCES

Cepeda-Gomez, R. and Olgac, N. (2011). An exact method for the stability analysis of linear consensus protocols with time delay. *IEEE Transactions on Automatic Control*, 56(7), 1734–1740.

Choe, C.U., Dahms, T., Hövel, P., and Schöll, E. (2010). Controlling synchrony by delay coupling in networks: from in-phase to splay and cluster states. *Physical Review E*, 81(2), 025205.

Coombes, S. (2008). Neuronal networks with gap junctions: a study of piecewise linear planar. *SIAM Journal on Applied Dynamical Systems*, 7(3), 1101–1129.

D'Huys, O., Fischer, I., Danckaert, J., and Vicente, R. (2011). Role of delay for the symmetry in the dynamics of networks. *Physical Review E*, 83(4), 046223.

Engelborghs, K., Luzyanina, T., and Samaey, G. (2001). DDE-BIFTOOL v. 2.00: a Matlab package for bifurcation analysis of delay differential equations. Technical Report TW-330, Department of Computer Science, Katholieke Universiteit Leuven, Belgium.

Insperger, T. and Stépán, G. (2011). *Semi-discretization for Time-delay Systems: Stability and Engineering Applications*, volume 178 of *Applied Mathematical Sciences*. Springer.

Izhikevich, E.M. (1998). Phase models with explicit time delays. *Physical Review E*, 58(1), 905–908.

Lin, P. and Jia, Y. (2009). Consensus of second-order discrete-time multi-agent systems with nonuniform time-delays and dynamically changing topologies. *Automatica*, 45(9), 2154–2158.

Meng, Z., Ren, W., Cao, Y., and You, Z. (2011). Leaderless and leader-following consensus with communication and input delays under a directed network topology. *IEEE Transations on Systems, Man, and Cybernetics – Part B*, 41(1), 75–88.

Montbrió, E., Pazó, D., and Schmidt, J. (2006). Time delay in the Kuramoto model with bimodal frequency distribution. *Physical Review E*, 74(5), 056201.

Newman, M., Barabasi, A.L., and Watts, D.J. (2006). *The Structure and Dynamics of Networks*. Princeton University Press.

Orosz, G., Moehlis, J., and Ashwin, P. (2009). Designing the dynamics of globally coupled oscillators. *Progress of Theoretical Physics*, 122(3), 611–630.

Roose, D. and Szalai, R. (2007). Continuation and bifurcation analysis of delay differential equations. In B. Krauskopf, H.M. Osinga, and J. Galan-Vioque (eds.), *Numerical Continuation Methods for Dynamical Systems*, Understanding Complex Systems, 359–399. Springer.

Stépán, G. (1989). *Retarded Dynamical Systems: Stability and Characteristic Functions*, volume 210 of *Pitman Research Notes in Mathematics*. Longman.